Chin. J. Astron. Astrophys. Vol. 4 (2004), No. 4, 320–334
( http://www.chjaa.org or http://chjaa.bao.ac.cn )

Chinese Journal of Astronomy and Astrophysics

# Spin Evolution of Neutron Stars in OB/X-ray Binaries *

Fan Zhang, Xiang-Dong Li and Zhen-Ru Wang

Department of Astronomy, Nanjing University, Nanjing 210093
zfastro@nju.edu.cn; lixd@nju.edu.cn; zrwang@nju.edu.cn

Received 2003 December 23; accepted 2004 February 18

**Abstract** We have investigated the relation between the orbital period $P_{\rm orb}$ and the spin period $P_{\rm s}$ of neutron stars in OB/X-ray binaries. By simulating the time-development of the mass loss rate and radius expansion of a $20M_{\odot}$ donor star, we have calculated the detailed spin evolution of the neutron star before steady wind accretion occurs (that is, when the break spin period is reached), or when the OB star begins evolving off the main sequence or has filled its Roche lobe. Our results are compatible with the observations of OB/X-ray binaries. We find that in relatively narrow systems with orbital periods less than tens of days, neutron stars with initial magnetic field $B_0$ stronger than about $3\times10^{12}$ G can reach the break spin period to allow steady wind accretion in the main sequence time, whereas neutron stars with $B_0 < 3\times10^{12}$ G and/or in wide systems would still be in one of the pulsar, rapid rotator or propeller phases when the companion evolves off the main sequence or fills its Roche lobe. Our results may help understand the various characteristics of the observed OB/neutron star binaries along with their distributions in the $P_{\rm s}-P_{\rm orb}$ diagram.

**Key words:** binaries: close – stars: evolution – stars: pulsars – stars: supergiants – stars: winds, outflows

## 1 INTRODUCTION

High mass X-ray binaries (HMXBs) can be roughly divided into Be/X-ray and supergiant binary systems. The X-ray source often is a pulsar, and is powered by accretion of material provided by the optical companion star. In the supergiant systems, this can be achieved through incipient Roche-lobe overflow or stellar wind accretion, while in the Be/X-ray systems, generally, only the latter process occurs because of their wide orbits (see Bhattacharya & van den Heuvel (1991) for a review). The distribution of massive X-ray binaries in the spin period ($P_{\rm s}$) vs. orbital period ($P_{\rm orb}$) diagram was first studied by Corbet(1984), who noted a positive correlation between $P_{\rm s}$ and $P_{\rm orb}$ in the Be/X-ray binaries, while wind-fed and disk-fed supergiant/X-ray binaries respectively occupy the upper and left-lower parts of the diagram. The $P_{\rm s}\sim P_{\rm orb}$ correlation has been studied by many authors, e.g., Corbet (1984), Stella et al. (1986), and

* Supported by the National Natural Science Foundation of China.

Waters & van Kerkwijk (1989), usually in terms of equilibrium spin period $P_{\rm s} = P_{\rm eq}$ of the neutron star, at which the centrifugal force acting on the wind matter close to the magnetospheric boundary can just balance the gravitational force exerted by the neutron star. For supergiant systems in which the stellar wind is usually assumed to be radially expanding, the assumption of the equilibrium spin period requires a mass accretion rate two orders of magnitude lower than is observed (Stella et al. 1986). It has therefore been suggested that the present distribution of wind-fed supergiant/X-ray binaries may result from an earlier evolutionary phase when the companion star was still on the main-sequence and its wind was much weaker (Waters & van Kerkwijk 1989). It needs to be examined, however, whether there is sufficient time for the neutron star to spin down to the observed period through interaction with such a weak wind. Moreover, the recent discovery of two supergiant systems 2S0114 + 65 (Corbet, Finley & Peele 1999) and OAO 1657 − 415 (Chakrabarty et al. 2002), which have respective spin periods of 10008 s and 38 s challenges the conventional equilibrium period theory. Detailed calculations of spin evolution of the neutron star in a massive binary are desirable in order to understand the observations of various kinds of OB/neutron star binaries (e.g., supergiant/X-ray binaries, main-sequence OB/X-ray binaries and OB/radio pulsar binaries) and their distributions in the $P_{\rm s} - P_{\rm orb}$ diagram.

In the present paper, we study the spin evolution of a $1.4M_{\odot}$ neutron star in a binary with a $20M_{\odot}$ OB star until steady accretion occurs, taking into account the evolution of the OB star and the magnetic field decay in the neutron star. The theoretical model of the neutron star spin evolution and the input physical parameters used in the calculation are respectively described in Sects. 2 and 3. The results and an examination of the effect of different parameters on the spin evolution are described in Sect. 4. Finally, we discuss the application to the observations in Sect. 5.

## 2 NEUTRON STAR SPIN EVOLUTION

We consider a binary system consisting of a young neutron star and a massive OB type main-sequence companion star. We adopt the theoretical model of Davies & Pringle (1981) (hereafter DP81) to describe the interaction between the neutron star and the wind material, which always forms a quasi-static envelope surrounding the neutron star, with, however, some considerable modifications (see below). In the following sections, we use the subscripts a, b, c, and d to denote the different evolutionary stages of the neutron star, i.e., (a) pulsar phase, (b) rapid rotator phase, (c) supersonic propeller phase and (d) subsonic propeller phase.

### 2.1 General Considerations

Following its birth in a supernova explosion, the neutron star in a binary system first appears as a radio pulsar with a short spin period ($P_{\rm s} \sim 10 - 100$ ms), if its radiation is strong enough to expel the wind material outside the Bondi radius (Bondi & Hoyle 1944) $r_{\rm G} = 2GM_{\rm x}/{v_{\rm rel}}^2$ ($G$, the gravitational constant, $M_{\rm x}$, the neutron star mass and $v_{\rm rel}$, the wind velocity relative to the neutron star) or the radius of the light cylinder, $r_{\rm lc} = cP_{\rm s}/2\pi$. Magnetic dipole radiation and/or energetic particle emission induce a spin-down rate of

$$\dot{P}_{\rm a} = \frac{L_{\rm a}{P_{\rm s}}^3}{4\pi I} = 3.07 \times 10^{-8} \mu_{30}^2 {P_{\rm s}}^{-1} I_{45}^{-1} \ {\rm s\,yr^{-1}}, \tag{1}$$

where $\mu_{30}$ is the magnetic moment of the neutron star in units of $10^{30}$ G cm$^3$ and $I_{45}$ is its moment of inertia in units of $10^{45}$ g cm$^2$, and $L_{\rm a}$ is the pulsar luminosity (throughout this

paper, we adopt typical neutron star mass $M_{\rm x} = 1.4 M_{\odot}$ and radius $r_{\rm x} = 10^6$ cm).

Since the relative wind velocity is highly supersonic in OB/neutron star binaries, a bow shock can form around the pulsar (Frank, King & Raine 2002). The distance of the shock stagnation point from the pulsar is about

$$r_{\rm a} = \Big(\frac{L_{\rm a}}{4\pi c \rho_{\rm w} {v_{\rm rel}}^2}\Big)^{1/2} = 3.19 \times 10^{10} \mu_{30} {P_{\rm s}}^{-2} (\rho_{-17} v_8^2)^{-1/2} \ {\rm cm}, \tag{2}$$

where the ram pressure of the external wind is balanced by the radiation pressure of the relativistic pulsar wind ($\rho_{\rm w} = 10^{-17} \rho_{-17}$ g cm$^{-3}$ is the wind density, and $v_8 = v_{\rm rel}/10^8$ cm s$^{-1}$). The outer radius $R_{\rm a} \sim 10 r_{\rm a}$ in DP81 was incorrectly estimated from the relativistic pulsar wind without considering the circumstance of the supersonic relative wind from the optical companion. Recent study on bow shock by, e.g., Bucciatini & Bandiera (2001), shows that the distance from the head of the bow shock to the stagnation point is just about $1.4 r_{\rm a}$. Since the whole envelope should be behind the bow shock, we adopt $R_{\rm a} = \eta r_{\rm a}$ with $\eta \approx 1.4$ in our calculation.

The pulsar phase (a) ends when the wind plasma penetrates inside either the light cylinder radius $r_{\rm lc}$ or the Bondi radius $r_{\rm G}$. The corresponding transitional spin periods of $P_{\rm ab}$ and $P_{\rm ac}$ can be respectively obtained by equating $r_{\rm a} = r_{\rm lc}$ and $R_{\rm a} = r_{\rm G}$ (since the pressure gradient set up by gravity dominates first at the large radius), i.e.,

$$P_{\rm ab} = 1.88 \mu_{30}^{1/3} \rho_{-17}^{-1/6} v_8^{-1/3} \ {\rm s}, \tag{3}$$

$$P_{\rm ac} = 0.93 \eta^{1/2} \mu_{30}^{1/2} v_8^{1/2} \rho_{-17}^{-1/4} \ {\rm s}. \tag{4}$$

The rapid rotator phase (b) obtains if $P_{\rm ab} < P_{\rm ac}$, or

$$\mu_{30} > 1.01 \times 10^3 \eta^{-3} \dot{M}_{15}^{1/2} v_8^{-7/2}, \tag{5}$$

where $\dot{M} = 10^{15} \times \dot{M}_{15}$ g s$^{-1}$ is the mass inflow rate. Equation (5) shows that most of the neutron stars with magnetic fields stronger than about $10^{12}$ G would experience the rapid rotator phase (b) if $\eta \sim 10$ as estimated in DP81. However, if, instead, $\eta \sim 1.4$, then this can happen only for a highly magnetized neutron star. We will discuss this phase in detail in the following subsection.

Thus, if $v_8 \sim 1$, neutron stars with normal magnetic field strength will enter the supersonic propeller phase (c) directly from the pulsar phase (a). This belongs to what Illarionov & Sunyaev (1975) called the strong stellar wind case. During phase (c), the angular velocity $\Omega$ of the neutron star is large enough that, at the inner boundary of the envelope $r_{\rm c}$, $r_{\rm c}\Omega > c_{\rm s}(r_{\rm c}) \simeq v_{\rm ff}(r_{\rm c})$ (DP81), $c_{\rm s}$ being the sound speed and $v_{\rm ff}$, the free fall velocity. Several kinds of magnitude estimates for the spin-down rate of a magnetic neutron star rotating supersonically in an external medium are summarized in Davies et al. (1979). Some MHD simulation works including Romanova et al. (2003), have been done recently in which complex density structures near the magnetosphere are found, in general agreement with the simulation result of Wang & Robertson (1985). We therefore give up the assumption of the equation of the state, $P(r) \propto r^{-3/2}$, adopted in DP81, and use the density assumption at the inner radius proposed in Wang & Robertson(1985),

$$\rho = \rho_{\rm m} M_{\phi}^2, \tag{6}$$

where $\rho_{\rm m}(r) = \dot{M}/(4\pi r^2 v_{\rm ff}(r))$ is the mass density just outside the magnetosphere and $M_{\phi}(r) = \Omega r / c_{\rm s}(r)$ is the Mach number. From the local pressure-balance condition ${B_{\rm m}}^2/8\pi = \rho {c_{\rm s}(r_{\rm c})}^2$,

we obtain the inner radius of the envelope at phase (c),

$$r_{\rm c} = 4.73 \times 10^8 {P_{\rm s}}^{4/13} \mu_{30}^{4/13} \dot{M}_{15}^{-2/13} \ {\rm cm}. \tag{7}$$

The rate of outward energy flow at $r_{\rm c}$ is estimated by

$$L_{\rm c} = \frac{d}{dt}[4\pi {r_{\rm c}}^2 \delta f \rho {v_{\rm t}}^2/2] \,, \tag{8}$$

where, as in DP81, $\delta$ is the width of the shear layer at the magnetospheric boundary, $v_{\rm t}$ is the turbulent velocity; $f$ is a measure of departure from axisymmetry and can be approximated as 2/3 (Mineshige, Rees & Fabian 1991). At the magnetospheric boundary, $d\delta/dt = v_{\rm t}(r_{\rm c}) \sim c_{\rm s}(r_{\rm c})$. Inserting Eq. (6) in Eq. (8), we then have

$$L_{\rm c} = \frac{1}{3} \dot{M} (\Omega r_{\rm c})^2. \tag{9}$$

This expression is analogous to eq.[3.5] of Mineshige, Rees & Fabian(1991). Assuming all of the rotational energy loss is transferred into the outward energy flow, the spin down rate is

$$\dot{P}_{\rm c} \simeq 2.11 \times 10^{-6} {P_{\rm s}}^{21/13} \mu_{30}^{8/13} \dot{M}_{15}^{9/13} \ {\rm s\,yr^{-1}}. \tag{10}$$

Phase (c) ends when $r_{\rm c}$ reaches the corotation radius $r_\Omega \equiv (GM_{\rm x}/\Omega^2)^{1/3}$, or when the spin period has increased to the equilibrium period $P_{\rm eq}$,

$$\begin{aligned} P_{\rm eq} &= 2^{-1/7} (GM_{\rm x})^{-5/7} \mu^{6/7} \dot{M}^{-3/7} \\ &\approx 9.5 \mu_{30}^{6/7} \dot{M}_{15}^{-3/7} \, {\rm s}. \end{aligned} \tag{11}$$

The condition for the neutron star to enter the supersonic propeller phase (c) directly from the pulsar phase ($P_{\rm ac} < P_{\rm ab}$) limits the maximum possible equilibrium spin period in this strong stellar wind case to

$$P_{\rm eq} < 3.54 \times 10^3 \eta^{-18/7} v_8^{-3} \ {\rm s}. \tag{12}$$

When the centrifugal force can no longer balance the gravity, the falling plasma has to be accreted. The pulsar-propeller-accretor sequence is accepted as a general spin evolutionary process of neutron stars in wind-fed systems, but they can be spun down further until steady accretion induced by interchange instability occurs (Arons & Lea 1976). During this stage, $\Omega r < v_{\rm ff} \sim c_{\rm s}$, so it is called the subsonic propeller phase (d) in DP81;—this phase will be discussed below.

### 2.2 The rapid rotator phase

In the weak stellar wind case, the wind material from the OB star penetrates the light cylinder of the neutron star before it does the Bondi radius (Illarionov & Sunyaev 1975), and the rapid rotator phase (b) commences. We estimate the spin down power in this phase as in DP81, where the incoming plasma at the inner boundary $r_{\rm b}$ of the envelope is considered to be heated to be sonic $\Omega r_{\rm b} = c_{\rm s}(r_{\rm b}) \gg v_{\rm ff}(r_{\rm b})$. The derived spin down rate is

$$\dot{P}_{\rm b} = 2.71 \times 10^{-8} \mu_{30} \dot{M}_{15}^{1/2} v_8^{5/2} {P_{\rm s}}^2 \ {\rm s\,yr^{-1}}. \tag{13}$$

The rapid rotator phase lasts until the outer boundary $R_{\rm b}$ approaches the Bondi radius $r_{\rm G}$. We divide this phase into two sub-phases: phase (b1), during which $R_{\rm b} > r_{\rm b} \geq r_{\rm G}$; phase (b2), during which $R_{\rm b} \geq r_{\rm G} > r_{\rm b}$. Phase b1 ends when the inner radius $r_{\rm b} = (\mu^2/(8\pi\rho_{\rm w}{v_{\rm rel}}^2))^{1/6}$ reaches $r_{\rm G}$, or when

$$\dot{M}_{15} \geq 6.54 \times 10^{-7} \mu_{30}^2 v_8^7. \tag{14}$$

Note that the above condition is very sensitive to the relative wind velocity and is independent of the spin period of the neutron star.

The following phase (b2) ends when the outer radius $R_{\rm b} = r_{\rm b}[\Omega r_{\rm b}/c_{\rm s}(R_{\rm b})]^{1/2}$ reaches $r_{\rm G}$ (DP81), ie., when the spin period becomes

$$P_{\rm bc} \simeq 1.89 \mu_{30} \dot{M}_{15}^{-1/2} v_8^{1/2} \ {\rm s}, \tag{15}$$

where $c_{\rm s}(R_{\rm b}) \simeq v_{\rm rel}$ has been used.

The above division of the rapid rotator phase is very important in the calculation of the spin evolution of neutron stars. If Eq. (15) is used directly to estimate the time when the rapid rotator phase (b) ends, then there may exist a serious problem that under certain circumstances, $P_{\rm bc}$ can be reached before the condition (14) is satisfied. This paradox did not arise since the condition $r_{\rm b} < r_{\rm G}$, which is independent of the spin period, was neglected before. Thus, in the weak stellar wind systems, the transitional spin period $P_{\rm bc}$ and the spin down timescale estimated directly from it should be used with care.

For systems where the condition (14) can not be satisfied at the end of the main sequence, the neutron star would stay in phase (b1), where the incoming plasma are almost totally obstructed outside the magnetosphere. This is the so called "magnetic plough" regime in Toropina et al. (2001). Since the mass loss rate and the radius of the OB star evolve slowly in the main sequence, if the spin down rate (Eq. [13]) was applicable throughout the whole phase, the neutron star would be spun down to very large spin period in a few million years. However, the condition of $\Omega r_{\rm b} > v_{\rm rel}$ limits the spin period in this phase, i.e.,

$$P_{\rm b} < 218 \mu_{30}^{1/3} \dot{M}_{15}^{-1/6} v_8^{-11/6} \ {\rm s}. \tag{16}$$

At the end of phase b1 ($r_{\rm b} = r_{\rm G}$), $v_{\rm ff}(r_{\rm b}) = v_{\rm rel} \sim \Omega r_{\rm b}$ is satisfied. Inserting Eq. (14) into Eq. (16), we obtain the maximum possible spin period in this case,

$$P_{\rm bmax} \equiv P_{\rm eq}(t_{\rm b}) = 2.34 \times 10^3 v_8^{-3} \ {\rm s}, \tag{17}$$

where $t_{\rm b}$ is the time when the rapid rotator phase (b) ends. In this case, the neutron star will enter the subsonic propeller phase (d) directly from phase (b1).

On the other hand, neutron stars in systems where Eqs. (14) and (15) can be realized in the main sequence time have a chance of going through the whole rapid rotator phase before entering the supersonic propeller phase. The condition of ending phase (b1) limits the largest possible equilibrium spin period in such systems to

$$P_{\rm eq} < 4.25 \times 10^3 v_8^{-3} \ {\rm s}. \tag{18}$$

### 2.3 The Subsonic Propeller Phase

When the corotation velocity at the inner boundary of the envelope approaches the local Keplerian velocity, the propeller action ceases to function, allowing direct wind accretion (Stella et al. 1986). However, steady accretion induced by the interchange instability can not take place

unless two conditions are satisfied: (1) The temperature $T$ of the boundary is less than a critical value $T_{\rm cr} \lesssim 0.3T_{\rm ff}$ ($T_{\rm ff} = GM_{\rm x}m_{\rm H}/kr_{\rm m}$ the proton free-fall temperature, $m_{\rm H}$ the mass of the particle, $k$ the Boltzman constant); (2) cooling dominates heating at the magnetosphere (Arons & Lea 1976; Elsner & Lamb 1977). The former condition is for the onset of the Rayleigh-Taylor instability, which implies the largest density of $\rho_{\rm crit} \sim 7\rho_{\rm m}$ just outside the boundary (Elsner & Lamb 1984), and the latter is for the steady accretion flow across the boundary.

Prior to the onset of the instability, little plasma can penetrate into the magnetosphere and be accreted, so Compton cooling is ineffective, and the plasma cools mainly by bremsstrahlung. If the equilibrium spin period were reached in the main sequence time (during which $\dot{M}_{15} \approx 1$), the plasma would accumulate outside the magnetosphere, since the bremsstrahlung cooling timescale $t_{\rm br}$ is far longer than the free fall timescale $t_{\rm ff}$. Once the density of the plasma grows to about the critical value $\rho_{\rm crit}$, the magnetosphere would become Rayleigh-Taylor unstable and the matter is able to penetrate into the magnetosphere.

For a rotating neutron star, whether or not the penetrated material could be accreted onto the surface of the neutron star may also depend on the efficiency of the cooling just below the magnetopause. Following DP81 and assuming the penetrated matter is only heated by the turbulent convective motion, the bremsstrahlung cooling would dominate the heating when

$$\frac{{v_{\rm t}}^2/2/(r/v_{\rm t})}{{v_{\rm ff}}^2/t_{\rm br}} < 1, \tag{19}$$

in which the turbulent velocity $v_{\rm t} \simeq \Omega r_{\rm m}$ and $t_{\rm br} = 2 \times 10^{11} T^{1/2} {n_{\rm i}}^{-1}$ ($n_{\rm i}$ the number density of the ionic plasma). It should be noted that the accumulation of the plasma can hardly change the inner radius $r_{\rm d} = r_{\rm m} = (\mu^2/(2\dot{M}\sqrt{2GM_{\rm x}}))^{2/7}$ (Elsner & Lamb 1977), whilst the temperature $T$ and the number density $n_{\rm i}$ just before the penetration satisfy $T \simeq 0.3T_{\rm ff}$, and $B^2/8\pi = n_{\rm i}kT$. Combining these conditions with Eq. (19), we obtain the break spin period

$$P_{\rm br} = 138.42\dot{M}_{15}^{-5/7}\mu_{30}^{16/21}\ {\rm s}. \tag{20}$$

During the subsonic propeller phase (d), assuming the neutron star loses its rotational energy at the rate of $L_{\rm d} = 2\pi {r_{\rm d}}^2 v_{\rm t}(r_{\rm d})^3 \rho(r_{\rm d})$, the corresponding spin down rate is

$$\dot{P}_{\rm d} = \frac{\pi\mu^2}{4GM_{\rm x}I} \simeq 1.2 \times 10^{-4}\mu_{30}^2\ {\rm s\,yr^{-1}}. \tag{21}$$

Steady wind accretion onto the surface of the neutron star occurs when $P_{\rm s} > P_{\rm br}$. Since the accreted material possesses some angular momentum, the neutron star spin could be further changed during the accretion phase. However, both observations (Bildsten et al. 1997) and numerical calculations (Fryxell & Taam 1988) have shown that the efficiency of angular momentum transfer in wind accretion is quite low, with alternating short-term spin-up and spin-down. Thus one may expect that the present spin periods of wind-fed X-ray pulsars are not significantly different from the $P_{\rm br}$ achieved earlier. So we stop the calculation before steady accretion occurs, that is, when $P_{\rm br}$ is reached or when the optical star starts to evolve off the main sequence. In some narrow systems, Roche lobe overflow may happen when the optical star is on the main sequence. In this case we stop the calculation when the Roche lobe becomes filled.

### 2.4 Summary

We have discussed the spin evolution of neutron stars under radial wind from main-sequence massive stars, based on the model of DP81 with the following modifications: (1) In the pulsar

phase, the outer radius of the atmosphere is $R_{\rm a} \sim 1.4 r_{\rm a}$ (Bucciatini & Bandiera 2001), which is about ten times smaller than that estimated in DP81. Thus the rapid rotator phase proposed by DP81 is important only for highly-magnetized neutron stars. (2) In the rapid rotator phase, the condition of $r_{\rm b} = r_{\rm G}$ (i.e., Eq.[14]) is emphasized (this condition is independent of the spin evolution of the neutron star), showing that the end point of the rapid rotator phase and its characteristic timescale should be treated with care. (3) In the supersonic propeller phase, we use the density assumption proposed in Wang & Robertson(1985), instead of the equation of state as in DP81, to recalculate the spin down rate. (4) In the subsonic propeller phase, we recalculate the break spin period from the onset conditions of the Rayleigh-Taylor instability near the boundary of the magnetosphere.

The evolutionary sequences can be summarized as follows according to the magnetic moment of the neutron star at the end of the pulsar phase (a):

(1) For neutron stars with $\mu_{30} < 1.01 \times 10^3 \eta^{-3} \dot{M}_{15}^{1/2} v_8^{-7/2}$, a $\rightarrow$ c $\rightarrow$ d.

(2) If $1.01 \times 10^3 \eta^{-3} \dot{M}_{15}^{1/2} v_8^{-7/2} < \mu_{30} < 1.24 \times 10^3 \dot{M}_{15}^{1/2} v_8^{-7/2}$, a $\rightarrow$ b2 $\rightarrow$ c $\rightarrow$ d.

(3) For neutron stars with $\mu_{30} > 1.24 \times 10^3 \dot{M}_{15}^{1/2} v_8^{-7/2}$, if the magnetic field decays or the mass transfer rate rises quickly enough to make $r_{\rm b} = r_{\rm G}$ at early time on the main sequence, a $\rightarrow$ b1 $\rightarrow$ b2 $\rightarrow$ c $\rightarrow$ d; else then a $\rightarrow$ b1($\rightarrow$ c $\rightarrow$ d).

Given the wind velocity, all of the above spin evolutionary sequences can be displayed in the $P_{\rm s} - \mu^{-2}\dot{M}$ diagram, see Fig. 1. The variables in the figure are all functions of time.

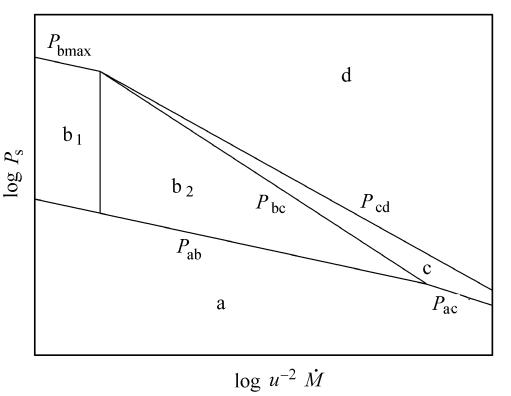


Fig. 1 Transition condition between different spin down phases in terms of $\log P_{\rm s}$ and $\log \mu^{-2}\dot{M}$. The transitional periods $P_{\rm ab}$, $P_{\rm bmax}$, $P_{\rm bc}$, $P_{\rm ac}$ and $P_{\rm cd} \equiv P_{\rm eq}$ are given by Eqs. (3), (16), (15), (4) and (11), respectively. The condition of ending phase (b1) (Eq.[14]) is independent of the spin evolution and is represented by a vertical line. The variables $P_{\rm s}$, $\mu$ and $\dot{M}$ are all functions of time, so there are four possible evolutionary processes as described in Sect. 2.4.

## 3 CALCULATION

In the case of main-sequence OB star/neutron star binaries, which we are interested in here, a knowledge of time development of the mass loss rate and the radius of the optical star is very important for the study of the spin evolution of the neutron star, since the former decides the end time of phase (b1) and the latter can tell us when the optical star fills its Roche lobe.

Using an updated version of the evolution code developed by Eggleton (1971), we simulate the evolution of a $20M_\odot$ star and trace its radius $R_2(t)$ and luminosity $L_2(t)$. The mass loss rate $\dot{M}_{\rm loss}(t) = -\dot{M}_2(t)$ is estimated (Nieuwenhuijzen & de Jager 1990) with

$$\log(-\dot{M}_2) = -14.02 + 1.24\log(L_2/L_\odot) + 0.16\log(M_2/M_\odot) + 0.81\log(R_2/R_\odot)\,.$$

The resulting $\dot{M}_{\rm loss}(t)$ and $R_2(t)$ are shown in Fig. 2, in which the part before the rapid expansion of the star can be fitted by

$$\dot{M}_{\rm loss}(t) = -\dot{M}_2(t) = \Big[3.39\times10^{-8} + 5.0\times10^{-9}\exp\Big(\frac{t}{2.28\times10^6}\Big)\Big] M_\odot\ {\rm yr}^{-1}, \tag{22}$$

and

$$R_2(t) = \Big[5.65 + 0.36\exp\Big(\frac{t}{2.46\times10^6}\Big)\Big] R_\odot\,. \tag{23}$$

These expressions hold for $t < 7.874\times10^6$ yr. Although the real evolution of the OB star in the binary system may be different from the single star, the main characteristics of the evolution would not be influenced significantly before luminous accretion occurs.

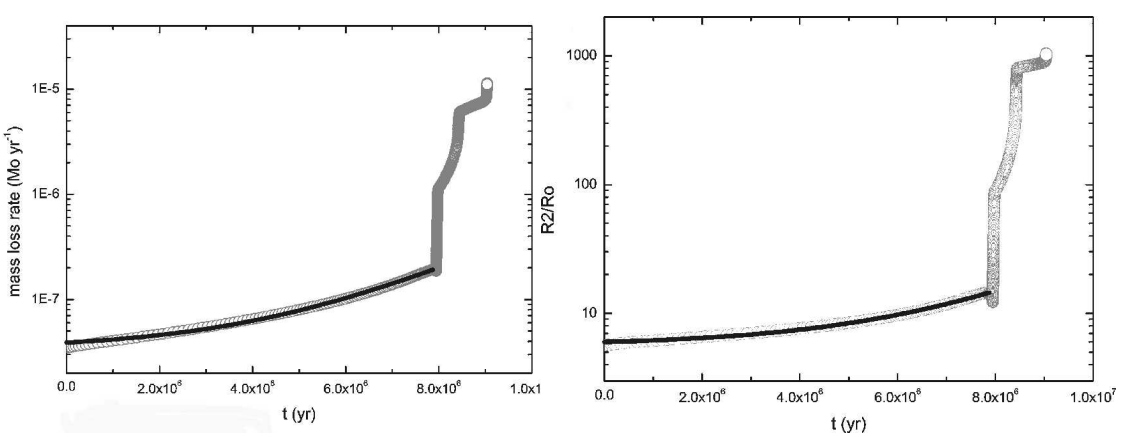


Fig. 2 Time development of the mass loss rate and the radius of a $20M_\odot$ star. The simulated results are represented by grey open circles, among which the part in the main-sequence can be fitted by Eqs. (22) and (23) for $\dot{M}_{\rm loss}(t)$ and $R_2(t)$, respectively, as shown by the thick black lines.

Assume that the wind lost from the optical star escapes totally from the system (the amount of captured wind material is very small), taking away a fraction $\zeta$ of the specific angular momentum of the optical star, the orbital separation $a$ of the binary will evolve as

$$\dot{a} = 2a\Big[-\frac{\dot{M}_2}{M_2} + \frac{1}{2}\frac{\dot{M}_2}{M_{\rm x}+M_2} + \zeta\frac{\dot{M}_2 M_{\rm x}}{M_2(M_{\rm x}+M_2)}\Big]\,. \tag{24}$$

We adopt $\zeta = 1$ in the calculation (the case of $\zeta = 0$ is also calculated, but there is no significant difference from the result of $\zeta = 1$).

The Roche lobe radius $R_{\rm roche}$ of the optical star, the wind density $\rho_{\rm w}$ at the orbit of the neutron star and the mass capture rate $\dot{M}$ are computed as follows (Frank, King & Raine 2002):

$$R_{\rm roche} = a[0.38 + 0.2\lg(M_2/M_x)]\,, \tag{25}$$

$$\rho_{\rm w} = \dot{M}_{\rm loss}/(4\pi a^2 v_{\rm rel})\,, \tag{26}$$

$$\dot{M} = \pi {r_{\rm G}}^2 \rho_{\rm w} v_{\rm rel}\,, \tag{27}$$

in which the relative wind velocity $v_{\rm rel} = ({v_{\rm w}}^2 + {v_{\rm orb}}^2)^{1/2}$, the orbital velocity $v_{\rm orb} = (G(M_{\rm x} + M_2)2\pi/P_{\rm orb})^{1/3}$, and the radial wind velocity $v_{\rm w}$ from the OB star,

$$v_{\rm w} = v_\infty(1 - R_2/a)^\beta\,, \tag{28}$$

where the terminal wind velocity $v_\infty \sim 10^3\ {\rm km\,s^{-1}}$, and $\beta \sim 0.5-1$ (see Waters & van Kerkwijk (1989) and reference therein). We adopt $\beta = 0.75$ in our calculation.

The instantaneous values of $v_{\rm rel}$, $\dot{M}$ and $\mu$ determine the spin-down rate and the transition spin periods in different phases as described in Sect. 2. We adopt $\mu \sim B(r_{\rm x}){r_{\rm x}}^3/2$ and assume exponential field decay when the field strength is less than the critical quantum magnetic field ($\sim 4 \times 10^{13}\,{\rm G}$),

$$B(t) = B_0 \exp(-t/t_{\rm d}), \tag{29}$$

where $B_0$ is the initial surface magnetic field strength, and $t_{\rm d}$ is the field decay timescale. We assume $t_{\rm d} \sim 5 \times 10^8/B_{012}$ yr, where $B_{012} = B_0/10^{12}\,{\rm G}$, around the diffusion time of magnetic flux through the crust of the neutron star (Goldreich & Reisenegger 1992).

For super strong magnetic fields ($B_0 > 10^{14}\,{\rm G}$), we assume field decay by ambipolar diffusion or Hall drift mechanism (Goldreich & Reisenegger 1992)

$$B(t) = \frac{B_0}{(1 + \epsilon\alpha B_{013}^\alpha t_6)^{1/\alpha}}, \tag{30}$$

where $B_{013} = B_0/10^{13}\,{\rm G}$, $t_6 = t/10^6$ yr. For crustal Hall cascade, $\epsilon = 10$, $\alpha = 1$; for ambipolar diffusion, in the irrotational mode $\epsilon = 0.01$, $\alpha = 5/4$, and in the solenoidal mode $\epsilon = 0.15$, $\alpha = 5/4$ (Colpi, Geppert & Page 2000). When the magnetic field strength drops below the critical quantum field strength, it is assumed to change to the exponential field decay.

Given $R_2(t)$, $B(t)$ and the other input variables, the coupled differential equations for $M_2$, $a$, $P_{\rm s}$ are integrated numerically for various sets of parameters.

## 4 RESULTS

We show in Figs. 3–6 the calculated final stages of the neutron star when either of the two conditions is met: (1) the spin period reaches $P_{\rm br}$ (represented by asters in the figures); (2) the optical star fills its Roche lobe or evolves off the main sequence. For the latter case, the neutron star may still stay in one of the four phases defined in Sect. 2. We use squares, triangles, circles and diamonds to mark the star in the pulsar, rapid rotator, supersonic propeller and subsonic propeller phases, respectively; and we use filled (or open) symbols to indicate that the optical fills its Roche lobe (or evolves off the main sequence). Panels (a) of the figures display the final states of the neutron star and the spin periods, $P_{\rm s}$, for initial orbital periods between 1

and 250 d. Panels (b) give the time when steady accretion occurs (the "final time" hereafter, which also represents the whole spin-down time). These figures have been selected from a large sample of computed models covering the following range of parameters and initial conditions:

$v_\infty$: 1000, 2000 ($\mathrm{km\,s^{-1}}$)

$P_0$ (initial spin period): 0.01, 0.1, 1(s)

$B_0$: $10^{11}$, $10^{12}$, $3\times10^{12}$, $7\times10^{12}$, $10^{13}$, $3\times10^{13}$, $3\times10^{14}$ (G).

Figure 3 shows the result with $v_\infty = 1000\ \mathrm{km\,s^{-1}}$ and $P_0 = 0.01$ s. It can be seen that, neutron stars with relatively weak initial magnetic field $B_{012} = 0.1$ are spun down very inefficiently in the pulsar phase. Most of them are still in this phase when the optical star begins evolving off the main sequence. In narrow systems of $P_{\rm orb} = 1 \sim 2$ d, the optical star even fills its Roche lobe when still on the main sequence. On the other hand, neutron stars with $3 < B_{012} < 30$ in orbital systems with $P_{\rm orb}$ less than a critical value $P_{\rm orb,\,max} \sim 10 - 100$ d (stronger $B_0$, larger $P_{\rm orb,\,max}$) can go through phases a, c, and d, and be spun down to $P_{\rm br}$ within the main-sequence life time. If $P_{\rm orb} > P_{\rm orb,\,max}$, the neutron star will still be in the propeller phase or even in the pulsar phase at the end of the main sequence time due to the smaller mass capture rate.

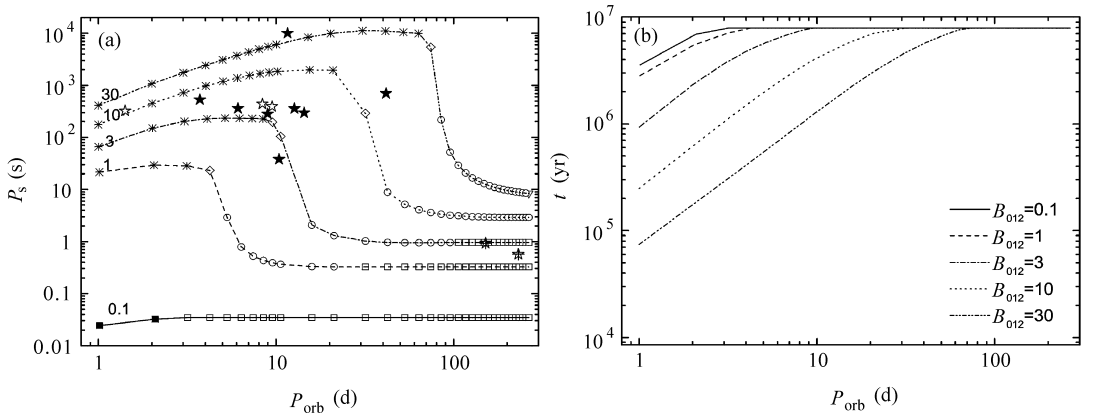


Fig. 3 (a) States of neutron stars in the $P_{\rm s} - P_{\rm orb}$ diagram just before accretion happens in a $1.4M_\odot$ NS + $20M_\odot$ OB star binary system. We adopt $v_\infty = 1000$ km s$^{-1}$, $P_0 = 0.01$ s, and $\dot{M}_2(t)$ by Eq. (22). Final states of neutron stars with $B_{012} = 0.1, 1, 3, 10, 30$ are joined by different line types indicated in Fig. 3(b). Squares, circles and diamonds mark phases (a), (c) and (d), respectively; open (filled) symbols indicate that the primary begins evolving off the main sequence (fills its Roche radius). Neutrons stars which can reach $P_{\rm br}$ in the main sequence time are represented by asterisks. For comparison, the observed distribution of wind-fed SG/X-ray binaries (filled pentacles), possible main-sequence OB/X-ray binaries (open pentacles) and massive binary radio pulsars (plus inside pentacles) are drawn. (b) Time corresponding to the final states of neutron stars in the main-sequence life time limit ($\sim 7.874\times10^6$ yr), when either the Roche lobe is filled, or $P_{\rm br}$ is reached.

In Fig. 4, we adopt the same group of parameters as in Fig. 3 except that $\dot{M}_2(t)$ is five times larger. With this global enhancement of the mass loss rate, the wind plasma compresses the magnetosphere further in, which results in a smaller $P_{\rm ac}$, so even some of those with $B_{012} \sim 0.1$ can now enter the supersonic propeller phase. The larger mass loss rate leads to larger spin down rate in the supersonic propeller phase and smaller $P_{\rm br}$, so that neutron stars with a wider

range of orbits can now reach relatively smaller $P_{\rm br}$ within the main-sequence life time.

We examine the effect of wind velocity on the spin evolution of neutron stars in Fig. 5, where $v_\infty = 2000$ km s$^{-1}$ is adopted, and other parameters are kept the same as in Fig. 3. Comparison with Fig. 3 is effected by up (down) triangles for the rapid rotator sub-phase b1 (or b2). The different evolutionary sequences are also reflected in their significantly different final times as shown in Fig. 5b. For example, in the case of $B_{012} = 30$, neutron stars with $P_{\rm orb} < 3$ d enter phase c and those with 3 d $\le P_{\rm orb} < 10$ d enter phase b2 directly from the pulsar phase; neutron stars with $P_{\rm orb} \ge 10$ d have to experience phase (b1), among which those with 10 d $< P_{\rm orb} < 80$ d may have been spun down to corotate with the outer wind material in this phase (represented by plus inside up triangle), and remain in this phase till the end of the main sequence.

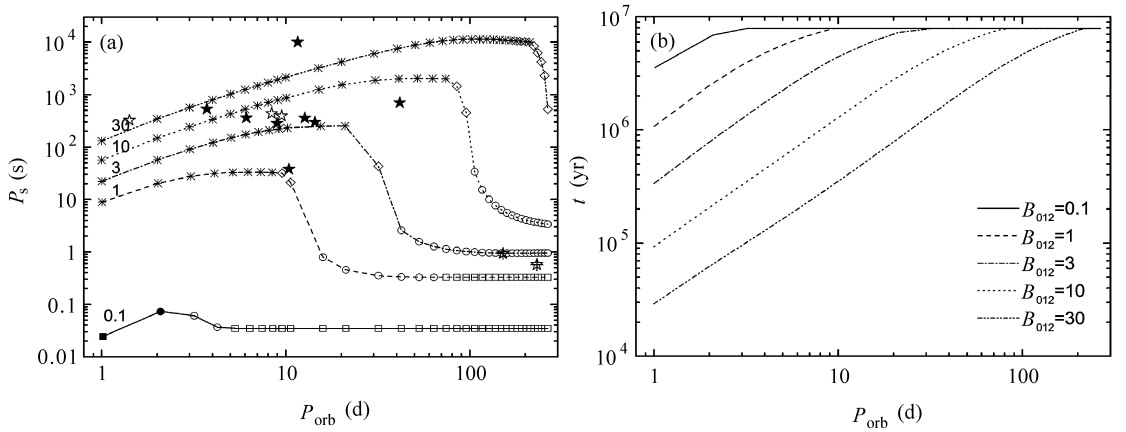


Fig. 4 Same as in Fig. 3, but for $\dot{M}_{\rm loss} = 5\times$ (Eq. (22)).

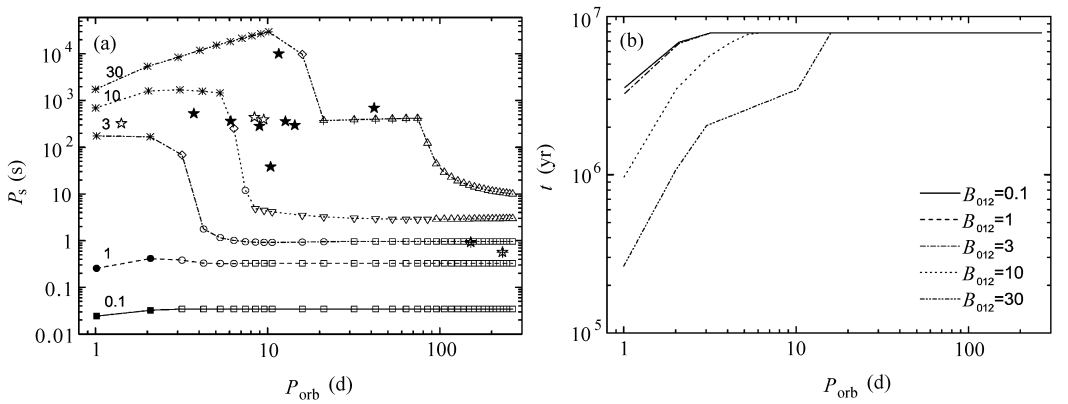


Fig. 5 (a) Same as Fig. 3, but for $v_\infty = 2000$ km s$^{-1}$. Symbols have the same meaning as in Fig. 3. New symbols of empty up (down) triangles in cases of $B_{012} = 10,\ 30$ mark neutron stars that are in phase (b1) (phase (b2)) when the primary evolves off the main sequence. In the case of $B_{012} = 30$, the symbols plus-inside-triangle mark stars which have spun down to $P_{\rm bmax}$ (corotating with the outer wind) in phase (b1), and remained in this phase till the companion evolved off the main sequence. (b) Corresponding time of the final states.

In Fig. 6, we draw the results of neutron stars with $B_{012} = 300$, for three forms of magnetic field decay in Eq. (30), assuming exponential field decay when $B_{12} \leq 30$. the other parameters are the same as in Fig. 3. To compare with the results of normal initial magnetic field, we also include the final states of neutron stars with $B_{012} = 30$. For the most efficient Hall cascade field decay, it is shown that except those with $P_{\rm orb} < 2$ d, the results of $B_{012} = 300$ are very similar to those of $B_{012} = 30$ in the $P_{\rm s} - P_{\rm orb}$ figure, but neutron stars with super strong initial magnetic fields get to $P_{\rm br}$ much sooner. For the Hall cascade field decay mode, the magnetic field strength of the neutron star decays so quickly that neutron stars enter the supersonic propeller phase (c) directly from the pulsar phase (a); whereas for the other two relatively slow field decay modes, the neutron stars have to experience the rapid rotator phase (b). The apparent changes of $P_{\rm br}$ and of the final time in the figure indicate different spin evolutionary processes analogous to those in Fig. 5.

Variations of $P_0$ can influence significantly the result with $B_0 < 3 \times 10^{12}$ G, since $P_{\rm ac}$ is thus comparable with $P_0$ if $P_0 \sim 1$ s. Otherwise, the influence of $P_0$ can be almost neglected because $P_{\rm ac}$ and $P_{\rm ab}$ are larger than $P_0$. Therefore, the results presented above can be safely used to indicate what is expected from the evolution of the binaries with $B_0 > 3 \times 10^{12}$ G.

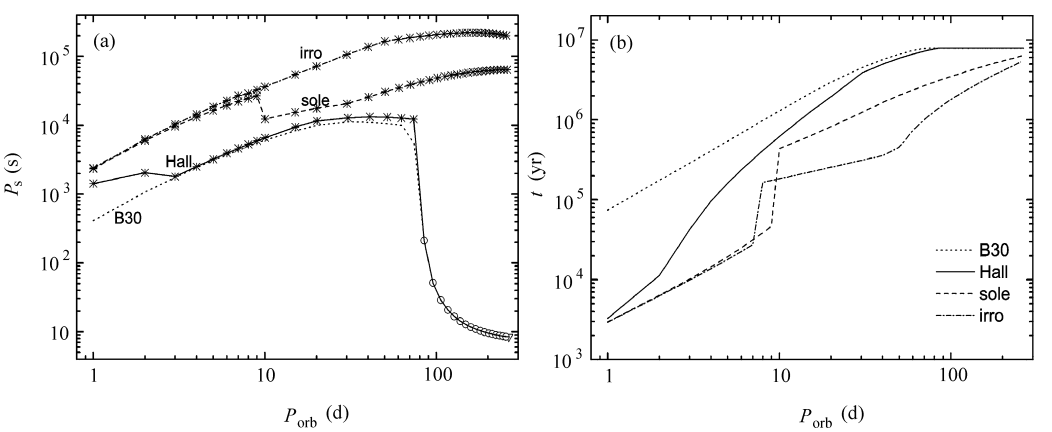


Fig. 6 (a) Final states of magnetars with initial magnetic field of $3 \times 10^{14}$ G just before accretion. Same parameters are adopted as in Fig. 3. Magnetic field decay by Hall cascade (solid line) , ambipolar diffusion of irrotational mode (dash-dotted line) and solenoidal mode (dashed line) are denoted by "Hall", "irro" and "sole", respectively, and compared with the exponential field decay in the case of $B_{012} = 30$ (dotted line). (b) Corresponding times of the final states.

## 5 DISCUSSION

We have calculated the spin evolution of a neutron star in a binary system with a massive OB companion star, taking into account the evolution of the latter and the magnetic field decay in the neutron star. A common feature of the results is that larger $B_0$ leads to larger $P_{\rm br}$ and relatively shorter spin-down time scale. Besides this, there exists a maximum orbital period $P_{\rm orb,\,max}$, below which neutron stars can reach $P_{\rm br}$ when the optical primary is still

on the main-sequence. Its magnitude depends on the mass loss rate, the wind velocity of the primary and the magnetic field strength of the neutron star. This explains the orbital period distribution of the observed persistent wind-fed HMXBs. The filled pentacles in Figs. 3–6 represent eight observed wind-fed supergiant/X-ray binaries, and the open pentacles represent three possible main sequence OB star/neutron star binaries, which are listed in Table 1. On the other hand, neutron stars with relatively weak surface magnetic field strength ($B_0 < 3\times10^{12}$ G) or/and in wide systems ($P_{\rm orb} > P_{\rm orb,\,max}$) may stay in the pulsar phase during the whole main-sequence stage. They would have a chance of being observed as massive binary radio pulsars in highly eccentric wide systems, since otherwise the radio signal would be scattered, dispersed or absorbed by the wind from the optical for most part of the orbit (Kaspi et al. 1994). PSR J0045 − 7319 (Kaspi et al. 1994) and J1740 − 3052 (Manchester 2001) are such examples. They are represented by plus-inside-pentacles in the $P_{\rm s} - P_{\rm orb}$ figure. PSR 1259 − 63 is another example but with a main-sequence Be optical star (Johnston et al. 1992).

**Table 1** Observed Wind-fed OB/Neutron Star Binaries and OB/Radio Pulsar Binaries*

| Source | $P_{\rm s}$ (s) | $P_{\rm orb}$ (d) | References |
|---|---|---|---|
| Vela X−1 | 283 | 8.96 | Liu et al. (2000) |
| 1E1145.1 − 6141 | 297 | 14.4 | Ray & Chakrabarty (2002) |
| X1538 − 522 | 529 | 3.73 | Liu et al. (2000) |
| SAX J2103.5 + 4545 | 358.61 | 12.68 | Liu et al. (2000) |
| XTE J1855 − 026 | 361 | 6.1 | Liu et al. (2000) |
| GX301 − 2 | 696 | 41.59 | Liu et al. (2000) |
| OAO1657 − 415 | 38 | 10.4 | Liu et al. (2000) |
| 2S0114 + 650 | 10008 | 11.6 | Liu et al. (2000) |
| 4U1907 + 097 | 438 | 8.38 | Liu et al. (2000) |
| RX J0050.7 − 7316 | 323 | 1.416 | Liu et al. (2000) |
| 4U2206 + 54 | 392 | 9.5 | Negueruela & Reig (2001) |
| PSR J0045 − 7319 | 0.926 | 51.17 | Kaspi et al. (1994) |
| PSR J1740 − 3052 | 0.57 | 231 | Manchester (2001) |

* The four groups of the data (from top down) correspond to the typical wind-fed supergiant/X-ray binaries, the special supergiant/X-ray binaries, possible main-sequence OB star/X-ray binaries and massive binary radio pulsars.

The observed wind-fed OB/neutron star binaries' distribution on the $P_{\rm s} - P_{\rm orb}$ diagram can be understood in terms of the break spin period along with their specific features as follows:

(1) For the wind-fed supergiant systems, e.g., Vela X-1, 1E 1145.1−6141, X1538−522, SAX J2103.5+4545 and XTE J1855−026, their positions on the $P_{\rm s}-P_{\rm orb}$ diagram can be understood in terms of the break spin period. Our results show that they are typical OB/neutron star systems with $B_0 \sim 3\times10^{12} - 10^{13}$ G, $v_\infty \sim 1000$ km s$^{-1}$ and $M_2 \sim 20M_\odot$. They got to the observed spin periods when the optical primary was at the late stage of the main sequence.

(2) Three special wind-fed supergiant systems, i.e. GX301−2, OAO1657−415, and 2S0114+650, which are widely scattered in the $P_{\rm s} - P_{\rm orb}$ diagram, can be understood in terms of their specific features. GX301 − 2, the widest binary among the supergiant systems with $P_{\rm orb} = 41.59$ d, could get to $P_{\rm br}$ in the main sequence time due to its very massive primary

star ($\sim 38 M_\odot$) and relatively slow wind velocity ($\sim 400$ km s$^{-1}$) (Kaper et al. 1995). The corresponding large mass loss rate from the primary compensates the effect of the wide orbit on the mass capture rate of the neutron star. OAO1657 − 415, which has the shortest spin period $P_{\rm s} = 38$ s and erratic spin-up and apin-down episodes (Chakrabarty et al. 2002), is among those that stay in the propeller phase when the optical primary evolves off the main sequence. The ensuing fast increasing mass loss rate of the primary star leads to the small $P_{\rm br}$ of the neutron star. 2S0114 + 650 (Corbet, Finley & Peele 1999) may have the strongest $B_0$ among the observed systems because of its longest spin period (Li & Van den Heuvel 1999). Generally $B_0 \geq 3 \times 10^{13}$ G is required by our model. Assuming early fast Hall cascade decay, if the magnetic field changes to exponential decay when the field drops to about the quantum critic $B \sim 4 \times 10^{13}$ G, the probability to observe neutron stars with magnetic field strength near the quantum critic value will be increased. Figure 5 shows a fast terminal wind velocity of about 2000 km s$^{-1}$ which is required in this case to make $P_{\rm br} \sim 10008$ s. However, by the equilibrium spin period theory, super strong magnetic field $B \sim 10^{15}$ G and relative slow magnetic field decay are needed to explain the 10 008 s spin period (Li & Van den Heuvel 1999). From our considerations in Sect. 2 (Eqs. (12) and (18)), it is easy to find that to reach such long equilibrium spin period, a wind velocity of less than about 750 km s$^{-1}$ is also required for the equilibrium spin period explanation.

(3) 4U2206+54, 4U1907+09, RX J1826.2−1450 and RX J0050.7−7316 are possibly active main-sequence massive star/neutron star systems (Negueruela & Reig 2001). The compact stars in these systems have seldom been observed to undergo outbursts and have low but persistent luminosities, implying they are wind accreting systems (Negueruela & Reig 2001). Compared with the supergiant binaries in group (1), they should have got to $P_{\rm br}$ earlier. Our calculations in Sects. 2 and 3 and the results in Figs. 3–5 show that the large mass capture rate due to high mass loss rate or relatively slow wind velocity can make the neutron star to spin down very efficiently in the propeller phase. However, since $P_{\rm br} \propto \dot{M}^{-5/7} \mu^{16/21}$, their positions in the $P_{\rm s} - P_{\rm orb}$ diagram, which are close to the supergiant systems, imply that the neutron stars in such systems may have stronger initial magnetic field strength. So we may expect that their optical primaries may have larger mass loss rate and/or slower wind velocity than those of the supergiant systems during main-sequence, and the neutron stars in these systems may have relatively stronger initial magnetic fields. With the evolution of the optical star, they would finally become supergiant/X-ray binaries. However, our results could not exclude other possible explanations for these systems. For example, RX J0050.7−7316 may be a triple system (Coe et al. 2002). Detailed optical observations and further studies of these systems are required. Pfahl, Rappaport & Podsiadlowski (2002) have explored the possibility of neutron stars accreting from the winds of the main-sequence optical stars to account for the low-luminosity, hard X-ray sources in the Galaxy. However, they did not consider the spin evolution of neutron stars in binary systems and the condition for the onset of wind accretion. Our calculations give further constraints on such systems.

**Acknowledgements** We are grateful to Yang Chen and P.-F. Chen for discussions of pulsar bow shock. We also acknowledge support from the National Natural Science Foundation of China grant 1007003 and grant NKBRSF-G19990754 of China Ministry of Science and Technology.

## References

Arons J., Lea S. M., 1976, ApJ, 207, 914
Bhattacharya D., van den Heuvel E. P. J., 1991, Phys. Rep., 203, 1
Bildsten L. et al., 1997, ApJS, 113, 367
Bondi H., Hoyle F., 1944, MNRAS, 104, 273
Bucciantini N., Bandiera R., 2001, A&A, 375, 1032
Chakrabarty D., Wang Z. X., Juett A. M., Lee J. C., 2002, ApJ, 573, 789
Coe M. J., Haigh N. J., Laycock S. G. T., Negueruela I., Kaiser C. R., 2002, MNRAS, 332, 473
Colpi M., Geppert U., Page D., 2000, ApJ, 529, L29
Corbet R. H. D., 1984, A&A, 141, 91
Corbet R. H. D., Finley J. P., Peele A. G., 1999, ApJ, 511, 876
Davies R. E., Fabian A. C., Pringle J. E., 1979, MNRAS, 186, 779
Davies R. E., Pringle J. E., 1981, MNRAS, 196, 209
Eggleton P. P., 1971, MNRAS, 151, 351
Elsner R. F., Lamb F. K., 1977, ApJ, 215, 897
Elsner R. F., Lamb F. K., 1984, ApJ, 278, 326
Frank J., King A. R., Raines D. J., 2002, Accretion Power in Astrophysics (3rd ed), Cambridge: Cambridge University Press
Fryxell B. A., Taam R. E., 1988, ApJ, 335, 862
Goldreich P., Reisenegger A., 1992, ApJ, 395, 250
Illarionov A. F., Sunyaev R. A., 1975, A&A, 39, 185
Johnston S. et al., 1992, ApJ, 387, L37
Kaper L., Lamers H. J. G. L. M., Ruymaekers E. et al., 1995, A&A, 300, 446
Kaspi V. M., Johnston S., Manchester R. N. et al., 1994, ApJ, 423, L43
Li X.-D., Van den Heuvel E. P. J., 1999, ApJ, 513, L45
Liu Q. Z., van Paradijs J., van den Heuvel E. P. J., 2000, A&A, 147, 25
Manchester R. N., 2001, MNRAS, 328, 17
Mineshige S., Rees M. J., Fabian A. C., 1991, MNRAS, 251, 555
Negueruela I., Reig P., 2001, A&A, 371, 1056
Nieuwenhuijzen H., de Jager C., 1990, A&A, 231, 134
Pfahl E., Rappaport S., Podsiadlowski P., 2002, ApJ, 571, L37
Ray P. S., Chakrabarty D., 2002, ApJ, 581, 1293
Romanova M. M., Toropina O. D., Lovelace R. V. E., 2003, ApJ, 588, 400
Stella L., White N. E., Rosner R., 1986, ApJ, 308, 669
Toropina O. D., Romanova M. M., Toropin Yu. M., Lovelace R. V. E., 2001, ApJ, 561, 964
Wang Y.-M., Robertson J. A., 1985, A&A, 151, 361
Waters L. B. F. M., van Kerkwijk M. H., 1989, A&A, 223, 196